Journal of South American Earth Sciences 88 (2018) 367–373

Contents lists available at ScienceDirect

Journal of South American Earth Sciences

journal homepage: www.elsevier.com/locate/jsames

New age in the geological evolution of the Cerro de Mercado Iron Oxide Apatite deposit, Mexico: Implication in the Durango apatite standard (DAP) age variability

Rodolfo Corona-Esquivel[a], Gilles Levresse[b,*], Jesús Solé[a,c], Fernando Henriquez[d], Teresa Pi[a,c]

[a] Instituto de Geología, Universidad Nacional Autónoma de México, CDMX, Mexico
[b] Centro de Geociencias, Campus, Juriquilla, UNAM, Mexico
[c] Laboratorio Nacional Geoquímica y Mineralogía, Universidad Nacional Autónoma de México, CDMX, Mexico
[d] Departamento de Ingeniería en Minas, Facultad de Ingeniería, Universidad de Santiago de Chile, Chile

ARTICLE INFO

Keywords:
DAP international standard
IOA deposit
K-Ar geochronology

ABSTRACT

Cerro de Mercado Iron Oxide Apatite deposit (CM-IOA) is known as a classical example of an IOA deposit worldwide and is also probably the most prolific locality in terms of gem-quality fluorapatite. The CM-IOA deposit is located in the Chupaderos Caldera Complex (CCC), a large rhyolitic volcanic center belonging to the Upper Volcanic Supergroup of Oligocene age. The main Cerro de Mercado IOA mineralization body is crosscut by a kilometer long rhyodacite dyke that acted as channelway for the rhyodacite flow. The rhyodacite dyke crosscuts all the volcanic sequence. K-Ar ages of this dyke range from ca. 28 to 27 Ma. Apatite in the Cerro de Mercado deposit appears in two different positions, (1) altered crystals intergrown with martite within massive mineralization, with or without diopside; and (2) on martite in degassing cavities and fracture zones, with accompanying chalcedony and calcite. Crystallization of the apatite phase was complete prior to the eruption of the overlying felsic flows of the Tinaja Member of the Cacaria Formation at ca. 31.44 Ma and preserve of potential late thermal event (McDowell et al., 2005). The mean ages reported by numerous and different isotopic methods for the fluorapatite DAP are coincident within the margins of uncertainty with the volcanic host rocks ages. But DAP ages reported present a significant variability of up to 8%. Such variability is also found in all dating technics applied in Durango Apatite (fission-track, U/Pb and (U-Th)/He ages) and suggest a thermal resetting related to the late volcanic event at 28-27 Ma.

1. Introduction

Cerro de Mercado Iron Oxide Apatite deposit (CM-IOA) is located in the City of Durango (Durango State, Mexico), at the boundary between the Sierra Madre Occidental volcanic province (SMO) at West, and Mesa Central at East. Cerro de Mercado deposit is known worldwide as a classical example of an IOA deposit and is also probably the most prolific locality in terms of gem-quality fluorapatite (Foshag, 1928; Young et al., 1969; Lyons, 1988; Corona-Esquivel and Henriquez, 2004; Henriquez and Corona-Esquivel, 2000). The « Durango apatite or DAP is relatively free of fluid and solid inclusions, and their crystals can easily attain a centimeter in diameter. These famous yellow-green fluorapatite crystals are instantly recognizable and commonly used as mineralogical (Mauthner and Ottaway, 2015), geochemical (Boyce and Hodges, 2005; Marks et al., 2012; Kusebauch et al., 2015; Holger et al., 2015; Mao et al., 2016; Sun et al., 2016; Chew et al., 2016; Müller and Anczkiewicz, 2016; Tacail et al., 2016; Gerin et al., 2017) and fission-track and (U-Th-Sm)/He thermochronometry (Zeitler et al., 1987, 2017; House et al., 1999; Ravenhurst et al., 2003; McDowell et al., 2005; Abdullin et al., 2014; Willett et al., 2017; Recanati et al., 2017; Li et al., 2018; Jonckheere et al., 2018; McDannell et al., 2018) standards. Zeitler et al. (1987) selected these apatites to set the base for thermochronometric studies. Even though the results showed straightforward and reproducible diffusive behavior of ^{4}He in the Durango fluorapatite (Zeitler et al., 1987), the conventional furnace and laser fusion (U-Th)/He dating of small DAP fragments yield apparent ages that vary by more than 8% (House et al., 1999). The fission-track (TF) variability ages could be reduced from 22 to 31 Ma to 32-28 Ma after analytical correction but do not disappear (Jonckheere et al., 2015). Several authors regularly comment the heterogeneous geochronological and isotopic behavior of the Durango apatite standard (i.e. House et al., 1999; Chew and Donelick, 2012; Abdullin et al., 2014).

* Corresponding author.
E-mail address: glevresse@geociencias.unam.mx (G. Levresse).

https://doi.org/10.1016/j.jsames.2018.09.014
Received 21 August 2018; Received in revised form 25 September 2018; Accepted 25 September 2018
Available online 28 September 2018
0895-9811/

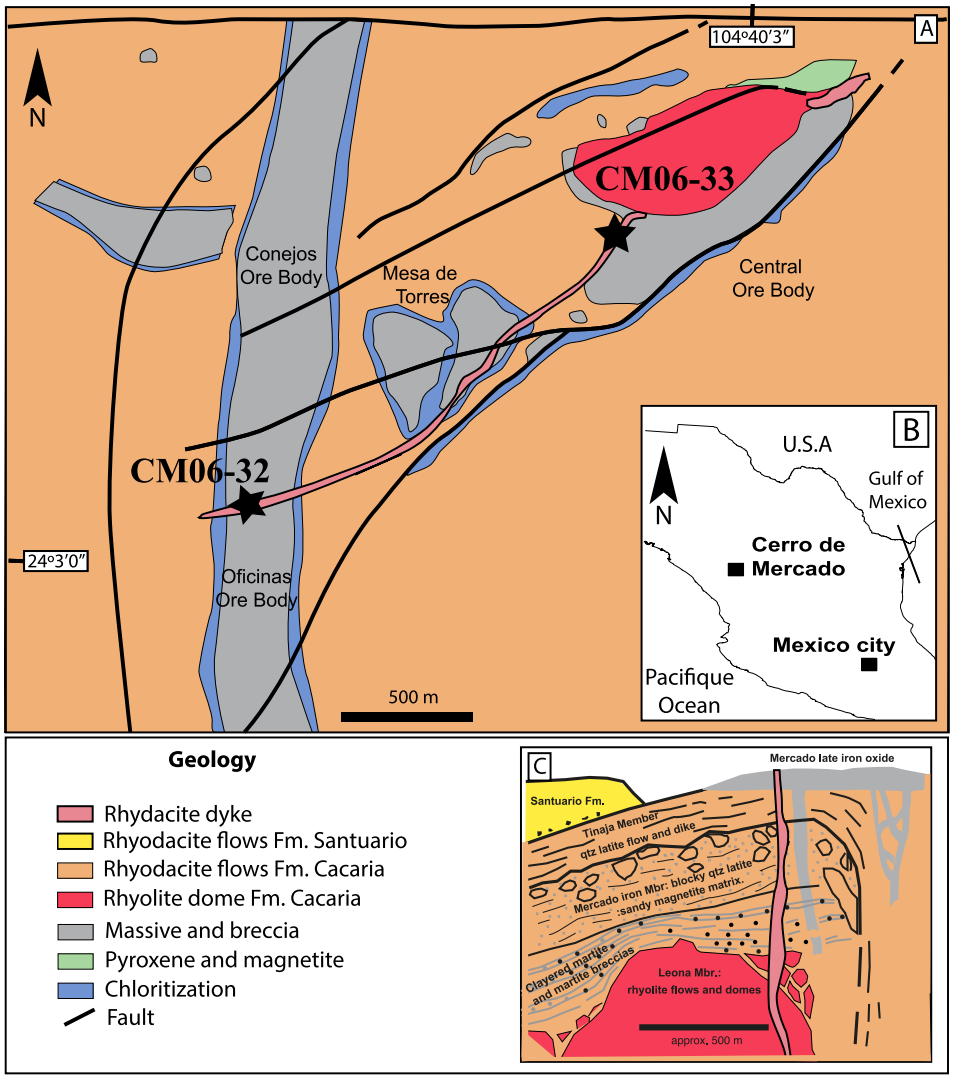

Fig. 1. (A) Simplified geological map of the Cerro de Mercado deposit. (B) Location of the Cerro de Mercado deposit in Mexico; (C) Stratigraphic sequence of the Cerro de Mercado (modified from McDowell et al., 2005). Black stars: dated samples localities.

The entire Chupaderos Caldera complex was formed in a surprisingly brief period of volcanic activity (less than 1 m.y., McDowell et al., 2005), pinning down the IOA mineralization and related apatite precisely within the analytical errors of the applied absolute dating method (McDowell et al., 2005).

The DAP is considered as an international geochronological and mineralogical standard Some relatively old geological reports on these apatites are available (Foshag, 1928; Young et al., 1969; Lyons, 1988; Henríquez and Corona-Esquivel, 2000; Corona-Esquivel and Henríquez, 2004) but none of them present detailed geological and mineralogical descriptions of the Cerro de Mecardo IOA deposit.

The aim of this paper is to summarize the geologic settings of the Cerro de Mercado IOA deposit, providing some new geological and paragenetical evidences and a new volcanic K-Ar age in order to bring novel geological contributions in the apatite geochronological heterogeneity discussion.

2. Geological setting

The Cerro de Mercado iron deposit is located in the central-eastern part of the Sierra Madre Occidental province (SMO; McDowell et al., 1997, 2005; Ferrari et al., 2007, 2013; Savage and Wang, 2012). The SMO constitutes the largest silicic igneous province in North America and the most recent event of this kind on Earth (Ferrari et al., 2007). The volcanic column is traditionally divided into two members known as Upper and Lower Volcanic Supergroups (McDowell et al., 2005, 2012; Ferrari et al., 2007, 2013; Savage and Wang, 2012). The Upper Volcanic Supergroup (UVS), that overlies the Lower Volcanic Complex (LVC) formed by a series of Late Cretaceous to early Eocene batholitic rocks and intermediate lavas (McDowell et al., 2005, 2012; Ferrari et al., 2007, 2013; Savage and Wang, 2012), is composed by a thick, late Eocene to early Miocene ignimbrite that covers most of the province. The UVS was emplaced between ca. 38-18 Ma, it is bimodal and made up mostly by rhyolitic ignimbrites, local rhyolitic domes and basaltic lavas intercalations. Detailed geochronological studies recognized two main flare-up events at ca. 34 - 28 Ma and ca. 24 - 18 Ma respectively (Ferrari et al., 2007, 2013). The Oligocene episode (ca. 34 - 28 Ma; including the Cerro de Mercado volcanic sequence and IOA member) forms up to 75% of the volcanic erupted volume. The Miocene ignimbritic pulse (ca. 24 - 18 Ma) is limited to the southwestern and western parts of the SMO and Baja California, (Ferrari et al., 2007, 2013). SMO in western Durango is composed by a plateau of flat lying ignimbrites, which appears to be unfaulted (Ferrari et al., 2007, 2013). On both flanks of this undeformed core, extensional fault systems tilted the ignimbrite succession in different directions, passing from crustal thickness of around 55 km in the ignimbrites core to 35 km in the

extended Eastern flank, close to CM-IOA deposit (McDowell et al., 2005, 2012; Ferrari et al., 2007, 2013).

The CM-IOA deposit sits in the Chupaderos Caldera Complex (CCC), a large rhyolitic volcanic center belonging to the UVS of Oligocene age (31.58 ± 0.16 to 31.44 ± 0.20 Ma, (Sanidine, $^{40}Ar/^{39}Ar$; McDowell et al., 2005). The caldera volcanic products rest unconformably on top of the folded Cretaceous limestone units, with locally some intercalations of discontinuous conglomerates (Ahuichila Conglomerate) and Eocene andesite flows (McDowell et al., 2005). The Chupaderos Caldera eruption originated an 8-km diameter central vent zone characterized by an autolithic breccia known as the Aguila unit. This eruption was followed by a collapse of the broader caldera area and the concomitant deposition of the overlying Cacaria Formation (Lyons, 1988). The latter is a heterogeneous mixture of volcanic flows, ash flow, lava dome, and volcanoclastic tuffs. In spite of its heterogeneity, it is formally divided into three members, (1) the Leona Member that comprises felsic flow domes, local ash flows and air-fall tuffs; (2) The Mercado Iron Member, that includes the iron oxide and apatite (IOA) ore deposits, associated to felsic plugs and breccias, emplaced over an erosional unconformity; and (3) The Tinaja Member formed by felsic flows that cover the main IOA ore body (Fig. 1; Lyons, 1988). A second major eruption at the CCC deposited the Santuario ignimbrite, a light gray crystal-vitric welded tuff over the Cacaria Formation. The eruption of the Santuario ignimbrite apparently occurred through a system of vents distributed throughout the caldera area, causing a small collapse. After this ignimbrite eruption, the activity of the caldera was more discreet. The Santa Maria Formation, a thin densely welded vitric ignimbrite, erupted from a 16-km-diameter collapse zone in the center of the caldera. It was followed by the eruption of the Caleras basalts located at the southern caldera margin (McDowell et al., 2005). $^{40}Ar/^{39}Ar$ absolute dating of Santuario and Aguila (sanidine, mono crystal; McDowell et al., 2005) indicates a short time interval of volcanic activity, from 31.59 ± 0.11 to 31.44 ± 0.20 Ma (McDowell et al., 2005). The main IOA mineralization body was crosscut by a kilometric long rhyodacite dyke that crosscuts all the volcanic sequence (Fig. 1; Corona-Esquivel and Henríquez, 2004). The contact between the dyke and the magnetite ore body is emphasized within the dyke by the presence of an up to 50 cm cooling rim (Fig. 2), coupled with a faint recrystallization halo affecting the magnetite ore body. This volumetrically important dyke is one of the few geological units with unknown absolute age in the CM-IOA deposit, and its possible influence and disturbance on the absolute ages already published remain unknown.

The IOA ore bodies are the result of subaerial volcanic processes that included the formation and eruption of volatile-rich iron oxide magmas, large scale fumarolic degassing and venting, and deposition of a conformable ash-like hematitic blanket in the surrounding area (Lyons, 1988; Naslund et al., 2002; Corona-Esquivel and Henríquez, 2004). Within the Chupaderos caldera all the other iron oxide ore deposits occur within the same general stratigraphic interval, and have been correlated as part of the "Mercado Iron Member" belonging to the Cacaria Formation (Lyons, 1988). Two different genetic processes have been proposed for this deposit. Some authors suggested an iron oxide-rich igneous melt that separated from a parental "oxide magma" in close relationship with the extrusion of silicic magmas, in a similar way as in El Laco deposit (Lyons, 1988; Naslund et al., 2002; Corona-Esquivel and Henríquez, 2004). Other, suggested the metasomatic replacement of previous volcanic rocks by massive oxide bodies triggered by hydrothermal fluids that vented-out onto the surface (Labarthe et al., 1987; Megaw and Barton, 1999; Barton et al., 2000).

The different ore bodies present a fairly simple mineralogy, made up by magnetite and hematite with minor apatite, and silica. Fe-oxide bodies are surrounded by an aureole of argillic alteration (Lyons, 1988; Corona-Esquivel and Henríquez, 2004). Hydrothermal alteration locally transforms magnetite and hematite to martite (Corona-Esquivel and Henríquez, 2004). The intimate association of the apatite and iron ore, and the occurrence of both during local magmatism is unmistakable. Apatite appears in two different positions, (1) altered crystal intergrown with martite within the massive mineralization, with or without diopside (Fig. 3A and B and Table 1); and (2) on top of martite in fumarolic degassing cavities and fracture zones, with chalcedony and calcite (Fig. 3C). The apatite crystallization overgrowths occur on the top and lateral limits of the magnetite ore body, probably from halogen-rich vapors (Dong, 2005). Crystallization of apatite was completed before eruption of the overlying felsic flows of the Santuario Formation (Figs. 1 and 2A-B; Corona-Esquivel and Henríquez, 2004). At present time, the mine workings allow to see that the emplacement of the deposit is structurally controlled by the intersection of two major faults of N-S and NE-SW trends that also host part of the breccia ore bodies (Figs. 1 and 2C).

Unaltered pyroxene related to primary apatite event have a homogeneous chemical composition (Table 1), crystallization temperatures ranging from 500 to 700 °C (Lindsley, 1983). The Cerro de Mercado IOA pyroxene present a very low OH content (< 0.001%) suggesting rather a magmatic than hydrothermal origin. Apatite chemical composition, in terms of F, Cl, SO_3, and OH, allow to classify them as F-apatite, poor in Cl, indicating a magmatic source (Corona-Esquivel and Henriquez, 2004). Cerro de Mercado magnetite samples are rich in V (up to 2400 ppm), and Mg (up to 2200 ppm) and poor in Ti (< 5000 ppm). Apatite, pyroxene and magnetite from Cerro de Mercado present similar composition than apatite, pyroxene and magnetite from the Cretaceous iron ores belt in Chile (Naslund et al., 2002) and Kiruna in Sweden (Nyström and Henríquez, 1994).

3. Experimental methods

Two dyke samples, the first located at the southwestern end and the second at the central part of the deposit (Fig. 1), were dated by the K-Ar method at the Noble Gas Laboratory of the Institute of Geology, Universidad Nacional Autónoma de México (Table 2). These samples were fragmented to a size of less than 2 mm with a steel disk breaker. Subsequently, they were sieved into two fractions, 500-400 μm and 400-250 μm to choose the most suitable for clean matrix separation. The fraction between 250 and 400 μm was used. The matrix separation was carried out with a Frantz magnetic separator, and finally by hand picking.

The measurements of K were made following the procedure using an X-ray fluorescence spectrometer, model Siemens 3000 XRF, calibrated with international reference materials (Solé and Enrique, 2001). The results have an uncertainty of 1%. The argon was measured by isotopic dilution with a mass spectrometer MM1200B operated under static vacuum (Solé, 2009). The samples were fused with an infrared (CO_2) laser in an ultra-high vacuum chamber. The gases were purified with a liquid nitrogen trap and two SAES solid state getters, one at room temperature and the other at 400 °C. The signal was acquired with an electron multiplier. The relative standard deviations of the ^{40}Ar, ^{38}Ar and ^{36}Ar isotopes are respectively < 0.1%, < 0.1% and < 0.5%. The data is reported with one standard deviation. The constants of Steiger and Jäger (1977) were used for the calculations.

Mineral phases and compositions were determined using a JEOL model 8900 Superprobe at the Binghampton University, NewYork, USA (Table 2).

4. New geochronological data of the Cerro de Mercado IOA deposit

The rhyodacite dyke did not receive sufficient attention by former authors while unraveling the age crosscutting relationships and succession in Cerro de Mercado iron deposit. For some authors, this dyke represents the feeding structure of the Oligocene Cacaria formation (Labarthe et al., 1987; Barton et al., 2000). Later, it was interpreted as representing the last magmatic event that occurred in the Caldera (Corona-Esquivel and Henríquez, 2004). This dyke crosscuts all the

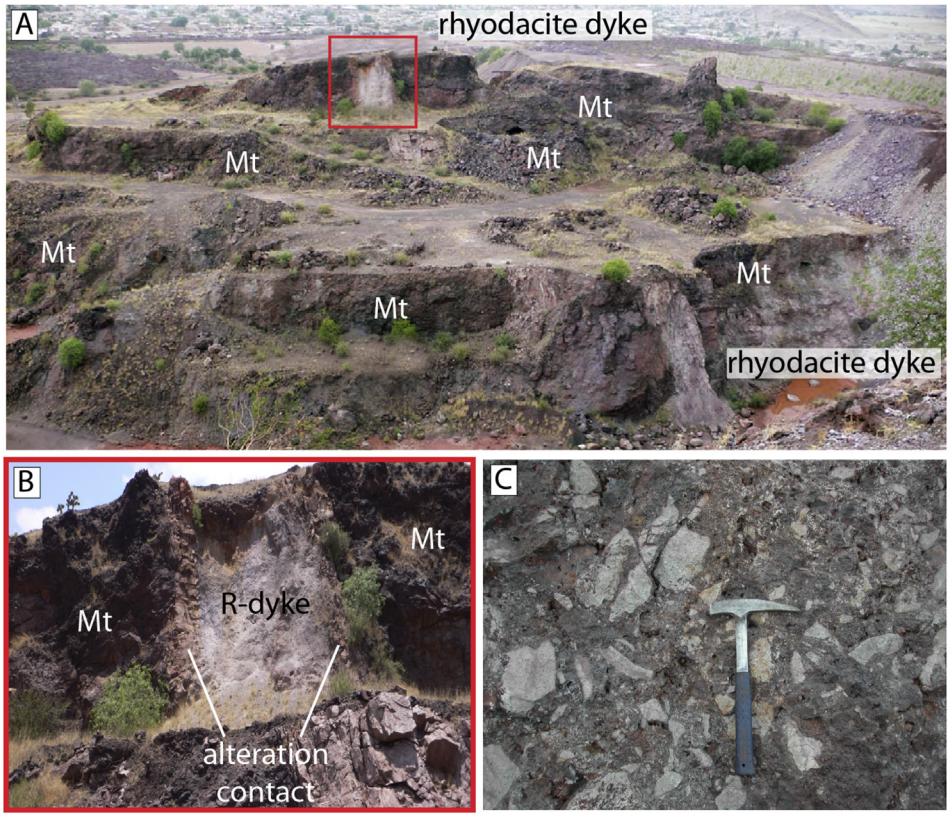

Fig. 2. (A): View of the central ore body in Cerro de Mercado IOA deposit, showing the rhyodacite dyke (this work) crosscutting the massive IOA mineralization. (B) Detail of the alteration rim provoked by the dyke intrusion into the IOA mineralization. (C) Detail of the Mercado Iron member composed by blocky latite breccia with magnetite cement. Mt: Magnetite; R-dyke: Rhyodacite dyke.

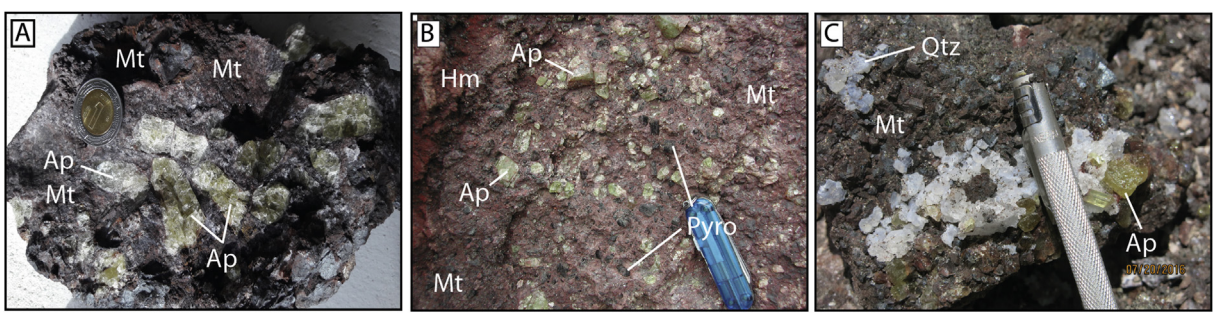

Fig. 3. Photographs of the two apatite occurrences in the Cerro del Mercado deposit, (A): apatite intergrown with martite in massive Fe-mineralization; (B): apatite and pyroxene intergrown with martite in massive Fe-mineralization; (C): apatite filling cavities and fracture zones with chalcedony and calcite. Mt: Magnetite; Ap: Apatite; Hm: Hematite; Qtz: Quartz.

Oligocene units, including the entire iron deposit, with a general NE-SW direction and for a length of 1350 m, being almost vertical throughout the entire strike, with a variable thickness between 6 and 9 m (Figs. 1 and 2; Corona-Esquivel and Henríquez, 2004). In the central part, it was not possible to verify its continuity as the outcrop is covered by mine dumps.

This dyke is light pink colored. Macroscopic observation allow to discern a porphyritic texture. The matrix is constituted by sub-millimeter crystals of plagioclase, K-feldspar and quartz. The plagioclase and K-feldspar phenocrysts are mainly euhedral to subhedral with sizes between 0.5 and 2 mm. Minute quartz crystals, biotite and diopside are also observed. Some xenoliths of magnetite-hematite are incorporated, when the rhyolitic dyke crosscut the Fe-oxides bodies.

The matrix fractions used for K-Ar dating consists of an inseparable mixture of potassium feldspar, plagioclase and quartz. It can be argued that the age of such "matrix" (Table 2) can be lower than the true age of the rock using the K-Ar chronometer. We cannot dismiss this possibility with absolute certitude, but it is not very probable due to the lack of later magmatism or diagenesis. In any case, it will be better to use the older of the two dates as a reference for the age of the dike.

The K-Ar results are presented in Fig. 4 and Table 2. The apparent ages for the rhyolitic dyke range from 27.3 to 28.1 Ma with analytical errors of ± 0.8–1.0 Ma.

5. Discussion

The origin of the Cerro de Mercado IOA deposit is intimately related to the Paleogene magmatism of the SMO, particularly with the development of the Caldera de Chupaderos (Lyons, 1988; McDowell et al., 2005; Corona and Henriquez, 2004). The age of the Cerro de Mercado volcanic sequence was established between 31.59 ± 0.11 and 31.44 ± 0.22 Ma (sanidine, $^{40}Ar/^{39}Ar$; McDowell et al., 2005) and the age of the late apatite related to the Fe mineralization based on its relationship with the Oligocene enclosing rock and fission-track (31.2 ± 0.2 Ma; apatite monocrystal, FT-LAICPMS, Abdullin et al., 2014, Fig. 4) and (U–Th–Sm)/He ages (31.03 ± 0.44 Ma (apatite monocrystal, McDowell et al., 2005, Fig. 4). In this geological history, the Cacarias formation overlies the IOA mineralization at

Table 1
Major element compositions of pyroxenes from Cerro de Mercado IOA mineralization.

Núm.	SiO2	Al2O3	Cr2O3	TiO2	FeO	MnO	MgO	CaO	Na2O	K2O	Wo	En	Fs	Identification
DM1701	53.9	0.8	0.0	0.0	8.1	0.1	13.4	21.9	1.6	0.0	46.6	39.8	13.6	Salite
DM1702	54.0	0.6	0.0	0.0	8.4	0.1	13.7	21.6	1.7	0.0	45.7	40.3	14.0	Salite
DM1703	53.9	0.2	0.0	0.1	8.1	0.2	13.8	22.3	1.2	0.0	46.4	40.1	13.5	Salite
DM1601	53.4	0.5	0.0	0.3	11.9	0.1	11.5	20.2	2.3	0.0	44.3	35.2	20.5	Salite
DM1602	54.1	0.4	0.0	0.1	7.7	0.1	13.9	21.9	1.5	0.0	46.3	40.9	12.8	Salite
DM1603	54.2	0.3	0.0	0.0	8.3	0.1	14.0	21.7	1.4	0.0	45.5	40.8	13.7	Salite
DM4401	53.1	0.7	0.0	0.3	10.2	0.1	12.4	21.1	1.7	0.0	45.5	37.2	17.3	Salite
DM4402	52.6	0.1	0.0	0.2	9.1	0.1	13.2	22.4	0.8	0.0	46.8	38.2	15.0	Salite
DM4403	53.7	0.2	0.0	0.0	8.9	0.1	13.1	21.6	1.5	0.0	46.2	38.8	15.0	Salite
DM4601	53.5	0.2	0.0	0.1	9.5	0.2	13.2	22.2	0.8	0.0	46.2	38.1	15.6	Salite
DM4602	53.1	0.7	0.0	0.3	9.7	0.1	12.6	20.4	1.8	0.0	44.8	38.6	16.7	Salite
DM4603	52.9	0.8	0.0	0.4	10.0	0.1	12.4	20.7	1.7	0.0	45.1	37.7	17.1	Salite
DM0401	53.5	0.5	0.0	0.2	9.6	0.1	13.0	21.3	1.6	0.0	45.3	38.5	16.2	Salite
DM402	53.5	0.5	0.0	0.2	9.8	0.1	13.0	21.4	1.4	0.0	45.3	38.3	16.4	Salite
DM403	53.9	0.2	0.0	0.2	9.4	0.1	13.3	21.8	1.0	0.0	45.7	38.8	15.5	Salite
DM1501	53.4	0.5	0.0	0.2	10.9	0.1	12.3	21.4	1.4	0.0	45.4	36.4	18.2	Salite
DM1502	53.5	0.4	0.0	0.1	10.2	0.1	12.7	21.6	1.3	0.0	45.7	37.3	17.0	Salite
DM1503	53.9	0.4	0.0	0.0	8.5	0.1	13.5	21.4	1.5	0.0	45.7	40.0	14.3	Salite
DM2701	52.4	0.7	0.0	0.1	13.7	0.2	9.6	20.3	2.4	0.0	45.6	30.1	24.3	Salite
DM2702	52.6	0.7	0.0	0.1	10.3	0.2	12.1	22.2	1.4	0.0	47.1	35.6	17.3	Salite
DM2703	52.8	0.9	0.0	0.1	11.0	0.1	11.4	21.3	1.9	0.0	46.4	34.6	19.0	Salite
DM1401	52.3	0.6	0.0	0.1	9.8	0.2	12.1	20.0	1.6	0.0	44.8	37.7	17.5	Salite
DM1402	52.9	0.9	0.0	0.3	10.6	0.1	12.0	20.6	1.8	0.0	45.2	36.6	18.2	Salite
DM1403	52.2	0.6	0.0	0.1	10.0	0.1	12.1	20.1	1.6	0.0	44.9	37.5	17.6	Salite
DM2101	51.0	1.4	0.0	0.4	15.1	0.2	8.9	19.5	2.6	0.0	44.4	28.4	27.2	Salite
DM2102	51.4	1.1	0.0	0.1	14.0	0.1	9.6	20.1	2.4	0.0	45.1	30.1	24.8	Salite
DM2103	51.1	1.3	0.0	0.4	15.3	0.1	9.0	19.6	2.7	0.0	44.4	28.2	27.4	Salite
DM2001	53.7	0.3	0.0	0.1	11.6	0.1	11.2	20.4	2.3	0.0	45.2	34.5	20.4	Salite
DM2002	53.7	0.3	0.0	0.2	10.1	0.1	12.0	20.5	2.1	0.0	45.3	37.0	17.6	Salite
DM2003	53.7	0.3	0.0	0.2	10.9	0.1	11.8	20.9	2.2	0.0	45.5	35.7	18.8	Salite

Table 2
K–Ar ages of the rhyodacite dyke.

Sample	Mineralogy	K (%)	$^{40}Ar^*$ (moles/g)	$^{40}Ar^*$ (%)	Age (Ma) (± 1σ)
CM06-32	matrix	3.30	$1.621 \cdot 10^{-10}$	87.3	28.1 ± 0.8
CM06-33	matrix	2.15	$1.027 \cdot 10^{-10}$	86.6	27.3 ± 1.0

31.44 ± 0.22 Ma, fix a minimum age of the DAP, and suggest that the DAP population is preserved from late thermal/geochemical modifications.

However, field relationship observations coupled with this new dyke K-Ar dating indicate that the CM-IOA Oligocene deposit is crosscut by a younger Oligocene volcanic event located at ca. 28-27 Ma. This fissural volcanism event is slightly younger, at local scale, in respect to the 30–31 Ma silicic explosive volcanism represented by the Chupaderos caldera. At a regional scale, it corresponds to the last large volcanic flare up of the SMO formation and marks the decrease in eruptive activity and heat anomaly observed between 28 and 25 Ma (Ferrari et al., 2007).

A detailed CM-IOA paragenetic sequence shows the occurrence of two different apatite formation events. The first apatite generation is coeval with the emplacement of the massive iron bodies, while the late second generation formed within fumarolic degassing fractures and voids with silica and carbonates. This late apatite event probably marks the end of the iron rich magmatic event by final degassing of volatiles and auto alteration of the previously deposited volcanic products. This last apatite generation is the most sought after for DAM due to their purity and very well crystalized shape. Both apatite generations occur between the Aguila and Santuario Oligocene volcanic formations, ca. 0.2 Ma (McDowell et al., 2005). The time between both apatite formation is too short to be analytically defined.

Fig. 4 is a compilation of the different ages reported for the CM-IOA volcanic host rocks (Fig. 4A; McDowell et al., 2005, and this study) and absolute apatite ages determined applying several analytical techniques (Fig. 4B–F). The $^{40}Ar/^{39}Ar$ ages for the volcanic host-rock formations of the Iron member define a thigh age range, comprised within the analytical error margin for the IOA (31.34 ± 0.01 and 31.51 ± 0.10 Ma; sanidine $^{40}Ar/^{39}Ar$ age, McDowell et al. (2005); Fig. 4A). This volcanic succession is crosscut by the late dyke at ca. 28-27 Ma (this study) which marks the end of the Oligocene volcanic activity in the region (Fig. 4A). Fig. 4B to G displays the published ages for the Durango fluorapatite using different analytical techniques. In general, the ages reported by different isotopic methods for volcanic rocks and DAP apatite are coincident within the margins of uncertainty and it can be summarized that to date the standard age for DAP apatite is still taken as 31.03 ± 0.44 (1σ) Ma (McDowell et al., 2005) or 31.4 Ma (Solé and Pi, 2005). But it is noteworthy that the apatite age range is quite wide, whatever the dating technique applied, from 33 to 27 Ma (Fig. 4). The FT-LAICPMS ages distribution range and errors are tighter than the conventional FT dating technique and are more comparable to the host rocks $^{40}Ar/^{39}Ar$ ages (from Fig. 4B and D). In brief, all dating techniques, including (U-Th)/He inter-laboratory age data (Fig. 4B–G), show a complex distribution that could be divided into two different populations, (1) a first population forming a well-defined family up to ca. 32 Ma, better defined in the U/Pb and conventional fission tracks methods and (2) a second population showing decreasing ages from ca. 31 to ca. 27 Ma (Fig. 4E). The same general decreasing evolution is observable in the distribution of the punctual FT-LAICPMS ages calculated for different DAP crystals and within a unique DAP crystal (Fig. 4G; modified from Abdullin et al., 2014; Jonckheere et al., 2015). Considering a fixed apatite composition (Boyce and Hodges, 2005; Chew et al., 2016; Mao et al., 2016; Sun et al., 2016), the most important impact factor for age modification should be the closing isotopic system temperatures, above 500 °C for the U/Pb system and above 150 °C for the (U-Th)/He system (Chew and Donelick, 2012). This discrete thermal event after apatite formation could induce some partial resetting in low temperature geochronometers like (U-Th)/He or apatite fission track. In the Cerro de Mercado IOA deposit, such late thermal event is represented by the late Oligocene fissural volcanism event at ca. 28-27 Ma, which precisely displays the same age than the younger - resetted? apatite ages

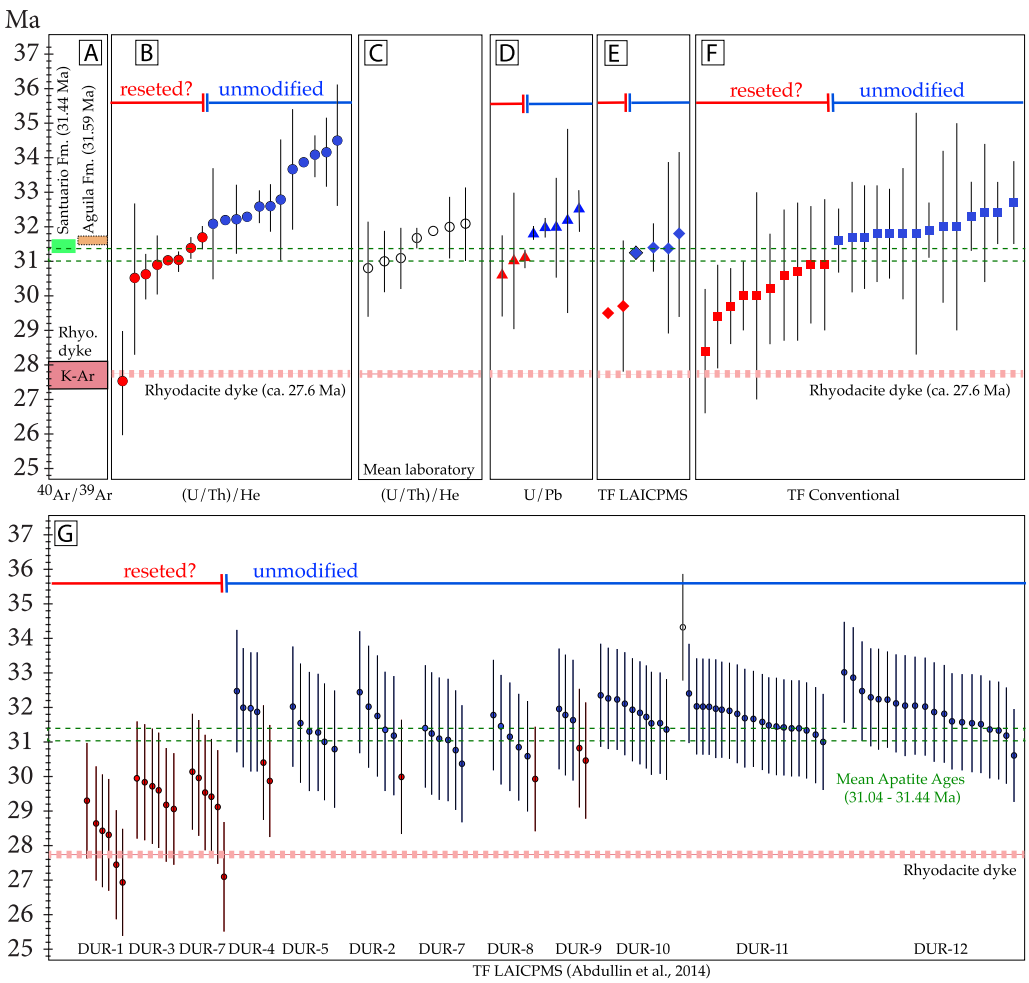

Fig. 4. Age comparison plot for Durango fluorapatite showing the single age variability and volcanic host-rocks bracketing ages; modified from Abdullin et al. (2014). (A) $^{40}Ar/^{39}Ar$ volcanic rocks, Sanctuario Fm. (green) and Carcaria Fm (orange; McDowell et al., 2005). and K-Ar age of the rhyodacite dyke (this study); (B) Red and blue circles: (U/Th)He DAP ages (McDowell et al., 2005; Farley, 2002; House et al., 2000; Solé and Pi, 2005); (C) open circles: (U/Th)He DAP mean age by laboratory, Waikato, CSIRO, Curtin, Tübingen, Arizona, Yale, Caltech; (D) Red and blue triangles: DAP U/Pb dating (Chew et al., 2011, 2014; Chew and Donelick, 2012; Li et al., 2012; Thomson et al., 2012; Cochrane et al., 2014); (E) Red and blue diamonds: Fission Track LA-ICPMS dating compilation (Hasebe et al., 2004; Hadler et al., 2009; Soares et al., 2014; Abdullin et al., 2014); (F) Red and blue squares: Fission Track conventional dating compilation (Hurford and Gleadow, 1977; Green, 1978; Märk et al., 1980; Jonckheere et al., 1993, 2015; Iunes et al., 2002); (G) Red and blue diamonds: Fission Track LAICPMS dating point in 12 different DAP crystals, (Abdullin et al., 2014). The green dotted area corresponds to the accepted DAP age variation (Abdullin et al., 2014 and references therein). Blue dots potentially unmodified ages; Red dots potentially resetted ages. (For interpretation of the references to color in this figure legend, the reader is referred to the Web version of this article.)

determined in the IOA-CM deposit. The relative temporal proximity of the late magmatic event described in this work to the primary age of the fluorapatite combined with the analytical errors makes somewhat difficult to identify with certitude the resetting, if present, as we observe in Fig. 4B–G. This late Oligocene volcanism is fissural and the thermal affectation induced to the DAP must be very heterogeneous at the deposit scale. As very few authors indicate the location of their apatites within the CM deposit it is so far impossible the estimate a size and intensity of the thermal affectation aureole.

6. Conclusions

The volcanic history of the Cerro de Mercado IOA deposit is directly related to the Chupaderos caldera, which strongly constrains the primary apatite crystallization age at 31.02 ± 0.22 Ma (McDowell et al., 2005). In this study we showed that the local volcanic history could be more complex and that a late volcanic event occurs in the Cerro de Mercado Fe district at ca. 27–28 Ma. Also we present field evidences of multistage apatite crystallization. The comparable age of the rhyolitic dyke and the (U-Th)/He and fission track younger ages determined in apatite suggest that the age variation range observed in DAP could be explained by a late thermal event at 28-27 Ma without considering potential bias in analytical techniques. The probable thermal affectation of the DAP population is very heterogeneous at the deposit scale.

Acknowledgments

Special thanks to Marina Vega, Juan Tomás Vásquez Pérez and Teresa Soledad Medina Malagón for their assistance at the CGEO laboratory. Funded by the UNAM-PAPIIT under grants IN-123202-2 and IN-115706-3 to Rodolfo Corona.

References

Abdullin, F., Solé, J., Solari, L., 2014. Datación mediante trazas de fisión y análisis multielemental con LA-ICP-MS del fluorapatito de Cerro de Mercado (Durango, México). Rev. Mex. Ciencias Geol. 31, 395–406.
Barton, M.D., Johnson, D.A., Zurcher, L., 2000. Phanerozoic iron-oxide (-REE-Cu-Au-U) sys- tems in southwestern North America and their origins. In: Roberts, M.D., Fairclough, M.C. (Eds.), Fe-oxide-Cu-Au Deposits: a Discussion of Critical Issues and Current Developments. EGRU Contribution 58. James Cook University, pp. 5–11.
Boyce, J.W., Hodges, K.V., 2005. U and Th zoning in Cerro de Mercado (Durango, Mexico) fluorapatite: insights regarding the impact of recoil redistribution of radiogenic ^{4}He on (U–Th)/He thermochronology. Chem. Geol. 219, 261–274.
Chew, D.M., Donelick, R.A., 2012. Combined apatite fission-track and U-Pb dating by LA-ICP-MS and its application in apatite provenance analysis. In: In: Sylvester (Ed.), Quantitative Mineralogy and Microanalysis of Sediments and Sedimentary Rocks, vol. 42. Mineralogical Association of Canada, pp. 219–247 Short Course.
Chew, D.M., Sylvester, P.J., Tubrett, M.N., 2011. U-Pb and Th-Pb dating of apatite by LA-ICPMS. Chem. Geol. 280, 200–216.
Chew, D.M., Petrus, J.A., Kamber, B.S., 2014. U–Pb LA-ICPMS dating using accessory mineral standards with variable common Pb. Chem. Geol. 363, 185–199.
Chew, D.M., Babechuk, M.G., Cogné, N., Mark, C., O'Sullivan, G.J., Henrichs, I.A., Doepke, D., McKenna, C.A., 2016. (LA, Q)-ICPMS trace-element analyses of Durango and McClure Mountain apatite and implications for making natural LA-ICPMS mineral standards. Chem. Geol. 435, 35–48.
Cochrane, R., Spikings, R.A., Chew, D.M., Wotzlaw, J.-F., Chiaradia, M., Tyrrell, S., Schaltegger, U., Van der Lelij, R., 2014. High temperature (N 350°C) thermochronology and mechanisms of Pb loss in apatite. Geochem. Cosmochim. Acta 127, 39–56.
Corona-Esquivel, R., Henríquez, F., 2004. Modelo magmático del yacimiento de Hierro Peña Colorada, Colima y su relación con la exploración de otros yacimientos de hierro en México, vol. 113. Universidad Nacional Autónoma de México, Instituto de

Geología, Boletín, pp. 97.
Dong, P., 2005. Halogen- Element (F, Cl and Br) Behavior in Apatites, Scapolite, and Sodalite: an Experimental Investigation with Field Applications. PhD thesis. pp. 234.
Farley, K.A., 2002. (U-Th)/He dating: techniques, calibrations, and applications. In: In: Porcelli, D., Ballentine, C.J., Wieler, R. (Eds.), Noble Gases in Geochemistry and Cosmochemistry: Washington, D.C, vol. 47. Geochemical Society and Mineralogical Society of America, pp. 819–844 Reviews in Mineralogy and Geochemistry.
Ferrari, L., Valencia-Moreno, M., Bryan, S., 2007. Magmatism and tectonics of the Sierra Madre Occidental and its relation with the evolution of the western margin of North America. In: In: Alaniz-Álvarez, S.A., Nieto-Samaniego, Á.F. (Eds.), Geology of México: Celebrating the Centenary of the Geological Society of México, vol. 422. Geological Society of America Special Paper, pp. 1–31.
Ferrari, L., López-Martínez, M., Orozco-Esquivel, T., Bryan, S.E., Duque-Trujillo, J., Lonsdale, P., Solari, L., 2013. Late Oligocene to middle Miocene rifting and syn-extensional magmatism in the southwestern Sierra Madre Occidental, Mexico: the beginning of the Gulf of California rift. Geosphere 9, 1161–1200.
Foshag, W.F., 1928. Mineralogy and geology of Cerro de Mercado, Durango, Mexico: U.S. National Museum Proceedings 74, 1–27.
Gerin, C., Gautheron, C., Oliviero, E., Bachelet, C., Mbongo Djimbi, D., Seydoux-Guillaume, A.M., Tassan-Got, L., Sarda, P., Roques, J., Garrido, F., 2017. Influence of vacancy damage on He diffusion in apatite, investigated at atomic to mineralogical scales. Geochem. Cosmochim. Acta 197, 87–103.
Green, P.F., 1978. Registration and Annealing of Fission Fragment and Heavy Ion Tracks in Crystals: Applications to Earth and Space Sciences. PhD tesis. University of Birmingham, Department of Physics, Birmingham, pp. 187.
Hadler, J.C., Iunes, P.J., Tello, C.A., Chemale Jr., F., Kawashita, K., Curvo, E.A.C., Santos, F.G.S., Gasparini, T.E., Moreira, P.A.F.P., Guedes, S., 2009. Experimental study of a methodology for fission-track dating without neutron irradiation. Radiat. Meas. 44, 955–957.
Hasebe, N., Barbarand, J., Jarvis, K., Carter, A., Hurford, A., 2004. Apatite fission-track chronometry using laser ablation ICP-MS. Chem. Geol. 207 (3), 135–145.
Henríquez, F., Corona-Esquivel, R., 2000. Yacimientos de fierro tipo Kiruna en México y comparación con yacimientos chilenos: Congreso Geológico Chileno, IX, Puerto Varas. Actas 2, 118–122.
Holger, T., Marks, M., Arzamastsev, A., Wenzel, T., Markl, G., 2015. Compositional variation of apatite from various host rocks: clues with regards to source composition and crystallization conditions. Neues Jahrbuch Mineral. Abhand. 192, 151–167.
House, M.A., Farley, K.A., Kohn, B.P., 1999. An empirical test of helium diffusion in apatite: borehole data from the Otway basin, Australia. Earth Planet Sci. Lett. 170, 463–474.
House, M.A., Farley, K.A., Stockli, D., 2000. Helium chronometry of apatite and titanite using Nd-YAG laser heating. Earth Planet Sci. Lett. 183, 365–368.
Hurford, A.J., Gleadow, A.J.W., 1977. Calibration of fission track dating parameters. Nucl. Track Detect. 1, 41–48.
Iunes, P.J., Hadler, N.J.C., Bigazzi, G., Tello, S.C.A., Guedes, O.S., Paulo, S.R., 2002. Durango apatite fission-track dating using length-based age corrections and neutron fluence measurements by natural thorium thin films and natural U-doped glasses calibrated through natural uranium thin films. Chem. Geol. 187 (3), 201–211.
Jonckheere, R., Mars, M., Van den Haute, P., Rebetez, M., Chambaudet, A., 1993. L'apatite de Durango (Mexique): analyse d'un minéral standard pour la datation par traces de fission. Chem. Geol. 103, 141–154.
Jonckheere, R., Tamer, M., Wauschkuhn, F., Wauschkuhn, B., Ratschbacher, L., 2018. Single-track length measurements of step-etched fission tracks in Durango apatite: Vorsprung durch Technik. Am. Mineral. 102 (5), 987–999.
Jonckheere, R., Van den haute, P., Ratschbacher, L., 2015. Standardless fission-track dating of the Durango apatite age standard. Chem. Geol. 417, 44–57.
Kusebauch, C., John, T., Whitehouse, M.J., Klemme, S., Putnis, A., 2015. Distribution of halogens between fluid and apatite during fluid-mediated replacement processes. Geochem. Cosmochim. Acta 170, 225–246.
Labarthe, G., Tristan, M.Y., Aguillon, A., 1987. Análisis de la Mina Cerro del Mercado, Dgo. Geomimet 150, 6–14.
Li, Q.L., Li, X.H., Wu, F.Y., Yin, Q.Z., Ye, H.M., Liu, Y., Tang, G.Q., Zhang, C.L., 2012. In-situ SIMS U-Pb dating of Phanerozoic apatite with low U and high common Pb. Gondwana Res. 21, 745–756.
Li, Q., Gleadow, A., Seiler, C., Kohn, B., Vermeesch, P., Carter, A., Hurford, A., 2018. Observations on three-dimensional measurement of confined fission track lengths in apatite using digital imagery. Am. Mineral. 103 (3), 430–440.
Lindsley, D.H., 1983. Pyroxene thermometry. Am. Mineral. 68, 477–493.
Lyons, J.L., 1988. Volcanogenic iron oxide deposits, Cerro de Mercado and vicinity, Durango, Mexico. In: In: Clark, K.F., Salas, G.A.P. (Eds.), A Special Issue Devoted to the Geology and Mineral Deposits of Mexico. Economic Geology, vol. 83. pp. 1886–1906.
Mao, M., Rukhlov, A.S., Rowins, S.M., Spence, J., Coogan, L.A., 2016. Apatite trace element compositions: a robust new tool for mineral exploration. Econ. Geol. 111 (5), 1187–1222.
Märk, T.D., Pahl, M., Vartanian, R., 1980. Fission track annealing and fission track age – temperature relationship in sphene. Nucl. Technol. 52, 295–305.
Marks, M.A.W., Wenzel, T., Whitehouse, M.J., Loose, M., Zack, T., Barth, M., Worgard, L., Krasz, V., Eby, N., Stosnach, Markl, G., 2012. The volatile inventory (F, Cl, Br, S, C) of magmatic apatite: an integrated analytical approach. Chem. Geol. 291, 241–255.
Mauthner, M., Ottaway, T., 2015. Gem apatite localities. Rocks Miner. 90 (3), 260–269.
McDannell, K.T., Zeitler, P.K., Janes, D.G., Idleman, B.D., Fayon, A.K., 2018. Screening apatites for (U-Th)/He thermochronometry via continuous ramped heating: He age components and implications for age dispersion. Geochem. Cosmochim. Acta 223, 90–106.
McDowell, F.W., McIntosh, W.C., 2012. Timing of intense magmatic episodes in the northern and central Sierra Madre Occidental, western Mexico. Geosphere 8 (6), 1505–1526.
McDowell, F.W., Roldán-Quintana, J., Amaya-Martínez, R., 1997. Interrelationship of sedimentary and volcanic deposits with Tertiary extension in Sonora, Mexico. Geol. Soc. Am. Bull. 109 (10) 1,349-1,360.
McDowell, F.W., McIntosh, W.C., Farley, K.A., 2005. A precise $^{40}Ar/^{39}Ar$ reference age for the Durango apatite (U–Th)/He and fission-track dating standard. Chem. Geol. 214, 249–263.
Megaw, P.K.M., Barton, M.D., 1999. The geology and minerals of Cerro de Mercado, Durango, Mexico. Rocks Miner. 74 (1), 20–29.
Müllerr, W., Anczkiewicz, R., 2016. Accuracy of laser-ablation (LA)-MC-ICPMS Sr isotope analysis of (bio)apatite – a problem reassessed. J. Anal. At. Spectrom. 31, 259–269.
Naslund, H.R., Henríquez, F., Nyström, J.O., Vivallo, W.Y., Dobbs, F.M., 2002. Magmatic iron ores and associated mineralization: examples from the Chilean high Andes and Coastal Cordillera. In: In: Porter, T.M. (Ed.), 2002 - Hydrothermal Iron Oxide Copper-gold & Related Deposits: a Global Perspective, vol. 2. PGC Publishing, Adelaide, pp. 207–226.
Ravenhurst, C.E., Roden-Tice, M.K., Miller, D.S., 2003. Thermal annealing of fission tracks in fluorapatite, chlorapatite, manganoanapatite, and Durango apatite: experimental results. Can. J. Earth Sci. 40, 995.
Recanati, A., Gautheron, C., Barbarand, J., Missenard, Y., Pinna-Jamme, R., Tassan-Got, L., Carter, A., Douville, E., Bordier, L., Pagel, M., Gallagher, K., 2017. Helium trapping in apatite damage: insights from (U-Th-Sm)/He dating of different granitoid lithologies. Chem. Geol. 470, 116–131.
Savage, B., Wang, Y., 2012. Integrated model of the crustal structure in the Gulf of California extensional province. Bull. Seismol. Soc. Am. 102, 878–885.
Soares, C.J., Guedes, S., Hadler, J.C., Mertz-Kraus, R., Zack, T., Iunes, P.J., 2014. Novel calibration for LA-ICP-MS-based fission-track thermochronology. Phys. Chem. Miner. 41, 65–73.
Solé, J., 2009. Determination of K-Ar ages in milligram samples using an infrared laser for argon extraction. Rapid Commun. Mass Spectrom. 23, 3579–3590.
Solé, J., Enrique, P., 2001. X-ray fluorescence analysis for the determination of potassium in small quantities of silicates minerals for K-Ar dating. Anal. Chim. Acta 440, 199–205.
Solé, J., Pi, T., 2005. An empirical calibration for ^{4}He quantification in minerals and rocks by laser fusion and noble gas mass spectrometry using Cerro de Mercado (Durango, Mexico) fluorapatite as a standard. Anal. Chim. Acta 535, 325–330.
Steiger, R.H., Jäeger, E., 1977. Subcommission on geochronology: convention on the use of decay constants in geo- and cosmochronology. Earth Planet Sci. Lett. 36, 359–362.
Sun, Y., Wiedenbeck, M., Joachimski, M.M., Beier, C., Kemner, F., Weinzierl, C., 2016. Chemicaland oxygen isotope composition of gem-quality apatites: implications for oxygen isotope reference materials for secondary ions mass spectrometry (SIMS). Chem. Geol. 440, 164–178.
Tacail, T., Télouk, P., Balter, V., 2016. Precise analysis of calcium stable isotope variations in biological apatites using laser ablation MC- ICPMS. J. Anal. At. Spectrom. 31, 152–162.
Thomson, S.N., Gehrels, G.E., Ruiz, J., 2012. Routine low-damage apatite U-Pb dating using laser ablation-multicollector-ICPMS. G-cubed 13, 1–23.
Willett, C.D., Fox, M., Shuster, D.L., 2017. A helium-based model for the effects of radiation damage annealing on helium diffusion kinetics in apatite. Earth Planet Sci. Lett. 477, 195–204.
Young, E.J., Myers, A.T., Munson, E.L., Conklin, N.M., 1969. Mineralogy and geochemistry of fluorapatite from Cerro de Mercado, Durango, Mexico. U. S. Geol. Surv. Prof. Pap. 650 (D), D84–D93.
Zeitler, P.K., Herczeg, A.L., McDougall, I., Honda, M., 1987. U-Th-He dating of apatite: a potential thermochronometer. Geochem. Cosmochim. Acta 51, 2865–2868.
Zeitler, P.K., Enkelmann, E., Thomas, J.B., Watson, E.B., Ancuta, L.D., Idleman, B.D., 2017. Solubility and trapping of helium in apatite. Geochem. Cosmochim. Acta 209, 1–8.